


Article

Integration of Illumina and PacBio HiFi Sequencing Reveals a Three-Linear-Molecule Mitogenome with RNA-Editing Sites and Phylogeny in Arrow Bamboo (*Fargesia qinlingensis*)

Hao Wu ^{1,†}, Xue Li ^{1,†}, Ke Qu ¹, Lele Yang ¹, Tao Su ^{1,*} , Lijun Yong ², Mei Han ^{1,*} and Fuliang Cao ³

- ¹ State Key Laboratory of Tree Genetics and Breeding, Co-Innovation Center for Sustainable Forestry in Southern China, Functional Genomics and Molecular Breeding Innovation Group for Bamboo, College of Life Sciences, Nanjing Forestry University, Nanjing 210037, China
- ² Foping National Nature Reserve, Foping Country, Hanzhong 723400, China
- ³ College of Forestry, Nanjing Forestry University, Nanjing 210037, China
- * Correspondence: sutao@njfu.edu.cn (T.S.); sthanmei@njfu.edu.cn (M.H.); Tel.: +86-1589-598-3381 (T.S.)
- † These authors contributed equally to this work.

Abstract: Arrow bamboo (*Fargesia qinlingensis*) is endemic to the Qinling Mountains and has remarkable adaptive resilience to changing climates. However, its complete mitogenome remains unknown. Using the Illumina and PacBio HiFi sequencing platforms, we found that the mitogenome assembly of the *F. qinlingensis* has a multi-branched skeleton comprising three linear molecules (M1, M2, and M3), with a length of 442,368 bp and a GC content of 44.05%. Thirty-five unique PCGs were identified in the complete mitogenome, including twenty-four core structural genes, eleven noncore structural genes, three rRNAs, and sixteen tRNAs. The GCU for alanine and CAA for glutamine represented the most significant frequency (RSCU = 1.55) in the codon usage preference. A total of 51, 28, and 14 SSRs were determined on M1, M2, and M3, respectively. The mitogenome contained 149 pairs of dispersed repeats with lengths greater than 30 bp, the most abundant of which were 82 forward and 67 palindromic repeats. A long repeat sequence (14,342 bp) was characterized in mediating mitogenome recombination. DNA transfer analyses suggested that 44 MTPTs (30,943 bp, 6.99%) originated from the plastome. Among the 482 potential C-U/T RNA-editing sites predicted in 35 PCGs, *ccmFn* (38 times) and *ccmC* (36 times) showed the highest frequency. Collinearity and phylogenetic trees revealed the close relationship between *F. qinlingensis* and *Bambusa oldhamii*. The primary features of the mitogenome of *F. qinlingensis* will help decipher the functional mitochondrial traits related to growth performance and climate resilience. Moreover, our findings provide insights into the evolution, environmental adaptation, and sustainable use of subalpine bamboo resources in the Qinling Mountains.

Keywords: *Fargesia qinlingensis*; mitogenome; HiFi sequencing; RNA-editing; stress resilience



Citation: Wu, H.; Li, X.; Qu, K.; Yang, L.; Su, T.; Yong, L.; Han, M.; Cao, F. Integration of Illumina and PacBio HiFi Sequencing Reveals a Three-Linear-Molecule Mitogenome with RNA-Editing Sites and Phylogeny in Arrow Bamboo (*Fargesia qinlingensis*). *Forests* **2024**, *15*, 1267. <https://doi.org/10.3390/f15071267>

Academic Editor: Claudia Mattioni

Received: 29 June 2024

Revised: 13 July 2024

Accepted: 18 July 2024

Published: 20 July 2024



Copyright: © 2024 by the authors. Licensee MDPI, Basel, Switzerland. This article is an open access article distributed under the terms and conditions of the Creative Commons Attribution (CC BY) license (<https://creativecommons.org/licenses/by/4.0/>).

1. Introduction

Plant cells integrate two energy-circulating systems involving mitochondria and plastids, both derived from prokaryotes of symbiotic ancestors [1]. Mitochondria house their own DNAs, RNAs, and ribosomes as semiautonomous and dynamic organelles, and undergo independent replication, transcription, and translation mechanisms, producing a few endogenous proteins [2,3]. They are the central cores of cellular respiration, and their unique structures and physiological properties allow them to have diverse functions, including generating ATP required for energy and regulating redox for photorespiration, which influences plant growth and stress acclimation [4,5]. Unlike nuclear genes, mitochondrial DNA in most terrestrial plants is often maternally inherited, contributing to population fitness and structural stability [6].

The plant mitogenome was previously considered a conventional and single, circular chromosomal structure based on the generally accepted notion in the scientific community. Nevertheless, emerging evidence suggests this to be an inaccurate and outdated concept [7]. Mitogenome size is not logically correlated with the number of annotated protein-coding genes (PCGs) but relies strongly on DNA mutation rates, which favor increased or reduced complexity and capacity in the mitogenome [8]. The horizontal transfer of homologous DNA fragments between plant genomes is critical to mitogenome evolution. RNA-editing events occur to maintain conserved proteins by generating new start or stop codons in amino acids, which affect translation, resulting in optimized protein length and function [9,10]. Investigating sequence variations and recombination events using the complete mitogenome offers unique advantages in reconstructing phylogenies and classification, providing new insights into disease and stress susceptibility, as well as lifespan extension during environmental and climate adaptation [11].

Bamboos, the tree-like grasses, are ecologically and economically important for their impact on wildlife habitats, human activities, biodiversity, and conservation. There are nearly 1700 recognized species categorized in the Bambusoideae subfamily of the Poaceae [12]. Three large tribes have been classified within the Bambusoideae, including a series of lineages from two woody bamboos (Arundinarieae and Bambuseae) and one herbaceous bamboo (Olyreae) [13]. Woody bamboos exhibit recalcitrance in their lignified culms, diversified leaves, and prolonged vegetative phases before flowering. They show a widespread distribution and altitudinal adaptation across most continents, mainly growing in Asia and America's temperate, subtropical, and tropical forests [14]. Within the Arundinarieae, the *Fargesia* is considered the largest genus, including approximately 90 bamboo species originating in mountain conifer forests of southwestern China [15]. The *Fargesia* genus features structural diversity and is a predominant component of subalpine forest ecosystems, representing dietary resources and providing shelter for many endangered animals, including the giant panda (*Ailuropoda melanoleuca*), the takin (*Budorcas bedfordi*), and the snub-nosed monkey (*Rhinopithecus bieti*) [16].

In the Qinling Mountains of China, endemic arrow bamboo (*F. qinlingensis* T. P. Yi & J. X. Shao) grows dominantly and is distributed on a large scale in high-altitude areas (>1800 m), exhibiting superior adaptation to extreme climates and provides tangible benefits for panda migration behavior and survival [17]. It also harbors biological functions related to the constituents and biodiversity of the subalpine bamboo population, ranging in elevation from 1800 to 3400 m [18]. Given the multiple roles of *F. qinlingensis* in the forest ecosystems of the Qinling Mountains, its slow growth patterns and delayed large-scale flowering due to climate change may pose massive risks to population succession despite its superior stress acclimation abilities [19]. Information on the theoretical basis of its ecological diversity and genetic evolution remains scarce due to its large genome size, complicated polyploidy, and mountain-adapted morphology [20]. Thus, exploring genomic patterns will provide comprehensive insights into phylogeny, sustainable conservation, and resilience to extreme subalpine climates in the *Fargesia* genus. Environmental cues induce retrograde redox signals in mitochondria, which trigger defensive responses in plants [21].

To date, very few high-quality bamboo mitogenomes have been reported in public databases, although it is known that they have undergone complicated and unusual evolutionary events across diverse families. In recent decades, technological advances in high-throughput sequencing have enabled the discovery of the entire mitogenomes of various plant species, providing essential insights into genetic diversity, evolution, and biogeography [22]. Given the few cases of the fast Illumina reads used for bamboo mitogenome assembly, high-quality mitogenomes are rarely available in the genus *Fargesia* [23]. Thus, dissecting the physiological functions of critical mitochondrial genes for stress/growth-related traits remains challenging. To achieve this goal, by integrating the Illumina and PacBio HiFi hybrid sequencing assays, the first high-quality mitogenome of the *F. qinlingensis* was resolved, revealing a structure of multi-branched conformation with three linear molecules (M1, M2, and M3), which have available NCBI accession GenBank

IDs (OP324798, OP324799, and OP324800). We further performed genome annotation, collinearity, and phylogenetic analyses to understand the conserved patterns and evolutionary significance of *F. qinlingensis* and other lineages in the Poaceae. Our findings provide a theoretical basis for elucidating the genetic evolution of mitochondrial DNA underlying climate resilience in subalpine bamboo.

2. Materials and Methods

2.1. Plant Materials, Sequencing, and Library Construction

Fresh leaves of *F. qinlingensis* were collected using liquid nitrogen (N) from the Foping National Nature Reserve, Qinling Mountain, Hanzhong City, Shaanxi Province, at an altitude of 2432 m (33°40′13″ N, 107°49′56″ E). Professor Tao Su and Dr. Yong Lijun identified the bamboo sample, and the voucher specimen was deposited in the herbarium of the Nanjing Forestry University (ID: ST20210502006). High-quality genomic RNA and DNA were isolated from 100 mg of N-frozen leaves using the Plant RNAprep Pure Kit (TianGen, Beijing, China) and CTAB methods [24]. RNA and DNA integrity (DNA \approx 1.8 and RNA \approx 2.0 under a ratio of OD 260/OD 280) and concentrations were determined via a Nanodrop 2000C UV/Vis spectrophotometer (Thermo, Waltham, MA, USA) and electrophoresis (GE) on a 1.5% agarose gel. The qualified RNA/DNA samples were sent to Wuhan Benagen Technology Co., Ltd., Wuhan, China (<http://en.benagen.com/>) for sequencing and library construction using the Illumina, NovaSeq 6000 (Illumina, San Diego, CA, USA) and PacBio HiFi, PACBIO SMRT (Sequel II) (Pacific Biosciences, Menlo Park, CA, USA) hybrid platforms.

2.2. De Novo Assembly of the Mitogenome and Gene Annotation

Illumina short-read sequencing data were first extracted using the GetOrganelle software (v1.7.7.1 2023.01.05) to generate a mitogenome unitig graph with default parameters [25]. The resulting PacBio HiFi long reads resolved repetitive regions and ensured consistency in the double bifurcating structure of the unitig graph. After removing single extended fragments from the plastome and nuclear genome, the mitogenome was visualized using the Bandage software (v0.9.0 2015.07.20) [26]. The PacBio HiFi data were further compared to the graphical fragments using the BWA software (v0.7.1 2017.11.07) to guarantee the accuracy of the assembled mitogenome [27]. Gene annotation was performed using the Geseq software (v2.03 2020.12.18), with *Arabidopsis* and barley (*Hordeum vulgare* L.) mitogenomes used as references [28]. Mitogenome tRNAs and rRNAs were annotated using the tRNAscan-SE software (v2.0.12 2021.09.20) and HS-BLASTN software (v2.15.0 2015.09.18), respectively [29,30]. The Apollo software corrected errors in each mitogenome annotation (v2.7.0 2023.01.04) [27].

2.3. Analysis of Codon Usage Preference and Repetitive Sequences

RSCU values (>1.2) indicated the specific codon usage preference among synonymous codons. Mitogenome PCGs were extracted using the PhyloSuite software (v1.2.3 2023.02.18), and the Mega X software (v10.2.5 2021.03) was used to analyze the PCGs for codon usage preference based on RSCU calculations [31,32]. The MISA (v2.1 2020.08.25), TRF (v4.09 2022.10.20), and REPuter (v1.0 2016.07.06) software programs were used to analyze the different sequence repeats, including SSRs, tandem repeats, and scattered repeats [27,33,34]. Collected sequence repeats were visualized using the RCircos package (v1.2.2 2021.12.19) [35]. The GetOrganelle software (v1.7.7.0 2023.01.05) generated different mitogenome conformations for the repeat region [25]. Specific sequence repeats were compared using the BWA software to determine whether the repeat region had long-spanning reads associated with the mitogenome primary structure [27].

2.4. Analysis of the Migration of MTPTs

Plastome assembly was conducted to identify mitochondrial plastid DNA (MTPT) fragments using the GetOrganelle software with default parameters [25]. Genes from

the plastome were annotated using the CPGAVAS2 online program (v2 2019.03.31) [36]. Homologous MTPTs were identified by comparing the mitogenome and the plastome using the HS-BLASTN software (cutoff = 1×10^{-5}) [29]. Transferred DNA sequences from the plastome were visualized using the RCircos package in the TBtools software (v2.070 2020.08.03) [37]. To confirm the MTPTs, the PacBio HiFi long reads were mapped by BLASTing the reference sequences using the BWA software [27]. The Tablet software (v1.21.02.08 2021.02.08) was used to construct a DNA sequence migration and homology map [38].

2.5. RNA-Editing Site Prediction and Experimental Evaluation

RNA-editing sites in all PCGs were analyzed using BWA with default parameters, and the BEDTools software (v2.31.1, <https://github.com/arq5x/bedtools2/releases> accessed on 8 November 2023) was subsequently employed to predict the editing sites in CDS with a setup of thresholds (coverage > 5, frequency ≤ 0.1 , and $p \leq 0.05$) [27,39]. SnapGene (www.snapgene.com) (v7.2.0 2024.09.19) was used to design primers for PCR applications to validate the RNA-editing sites in the selected PCGs. A Nanodrop 2000C UV/Vis spectrophotometer (Thermo, USA) was used to evaluate the sample quality. cDNA was synthesized via reverse transcription of RNA using the HiScript III First Strand cDNA Synthesis Kit (Yugong, China). The prepared PCR mixture was subjected to a Mastercycler[®] nexus PCR Thermal Cycler (Eppendorf, Hamburg, Germany) according to the manufacturer's instructions using a program of denaturation at 95 °C for 3 min (95 °C for 15 s, 54 °C for 12 s, 72 °C for 15 s) for 35 cycles, followed by a final extension at 72 °C for 5 min. The PCR-amplified products were subjected to GE analyses on a 1.5% agarose, followed by Sanger sequencing (Sangon, Shanghai, China).

2.6. Collinearity and Phylogenetic Tree Construction

Homologous DNA sequences (>500 bp) were collected as conserved collinear blocks to generate conserved multiple synteny blocks using the MCScanX package (<https://github.com/wyp1125/MCScanX>, accessed on 8 November 2023, vX 2013.11.11) [40]. Multiple mitogenomes were aligned and compared for phylogenetic analyses to explore the collinear relationships between genetically related species using the HS-BLASTN software [29]. The MAFFT software (v7.525 2024.03) was used for sequence alignments of multiple mitogenomes [41]. The MrBayes software (v3.2 2001.08.01) was used as a program for Bayesian phylogenetic estimation [42]. The PhyloSuite software was used to extract homologous PCGs among various complete mitogenomes of the selected species, and the iTOL software (v6.9 2021.07.02) was used to visualize the unrooted phylogenetic tree [43].

3. Results

3.1. Mitogenome Assembly and Configuration of *F. qinlingensis*

Mitogenome sequencing of *F. qinlingensis* was conducted using hybrid platforms, generating 50 Gb (average length: 150 bp) of Illumina short-read data and 10.03 Gb (average length: 15,670 bp) of PacBio HiFi long-read data, covering average genome depths of $1293.93\times$ and $126.49\times$ genome, respectively (Figure S1). Detailed BAM QC statistics for the mitogenome sequencing data are available in Table S1. Using the Bandage software, a draft mitogenome combined with six branch contigs (ctg1-ctg6) was initially assembled (Figure 1A). Ctg5 in the unitig graph, which contained a 14,342 bp repeat sequence, may have facilitated mitogenome recombination, leading to four different solution pathways (ctg4-ctg5-ctg6, ctg1-ctg5-ctg2, ctg4-ctg5-ctg2, and ctg1-ctg5-ctg6) and resultant conformational changes (Table S2 and Figure S2). Based on the highest supported number, the long-read collections of BLASTn were validated by mapping the reference sequence composed of ctg5 and its 500 bp flanking regions (Table S3). Subsequently, a multi-branched mitogenome sketch with the ctg1-ctg5-ctg6 path was primarily obtained and visualized, which included 54 key branch nodes linked to form the overlapping regions, long repetitive regions (recombination sequences) (red), and DNA sequences migrated from the plastome

(green) (Figure 1B,C, and Table 1). After resolving the duplicated regions based on the PacBio HiFi long-read sequencing data, the major assembled mitogenome of *F. qinlingensis* showed a specific multi-branched structure of 442,368 bp, with a GC content of 44.05% (Figure 1B). The complete mitogenome conformation was simplified into three linear molecules with overlapping regions: 208,716 bp for M1 (GC = 44.21%, red), 160,262 bp for M2 (GC = 44.06%, yellow), and 73,390 bp for M2 (GC = 43.57%, blue) (Table S4).

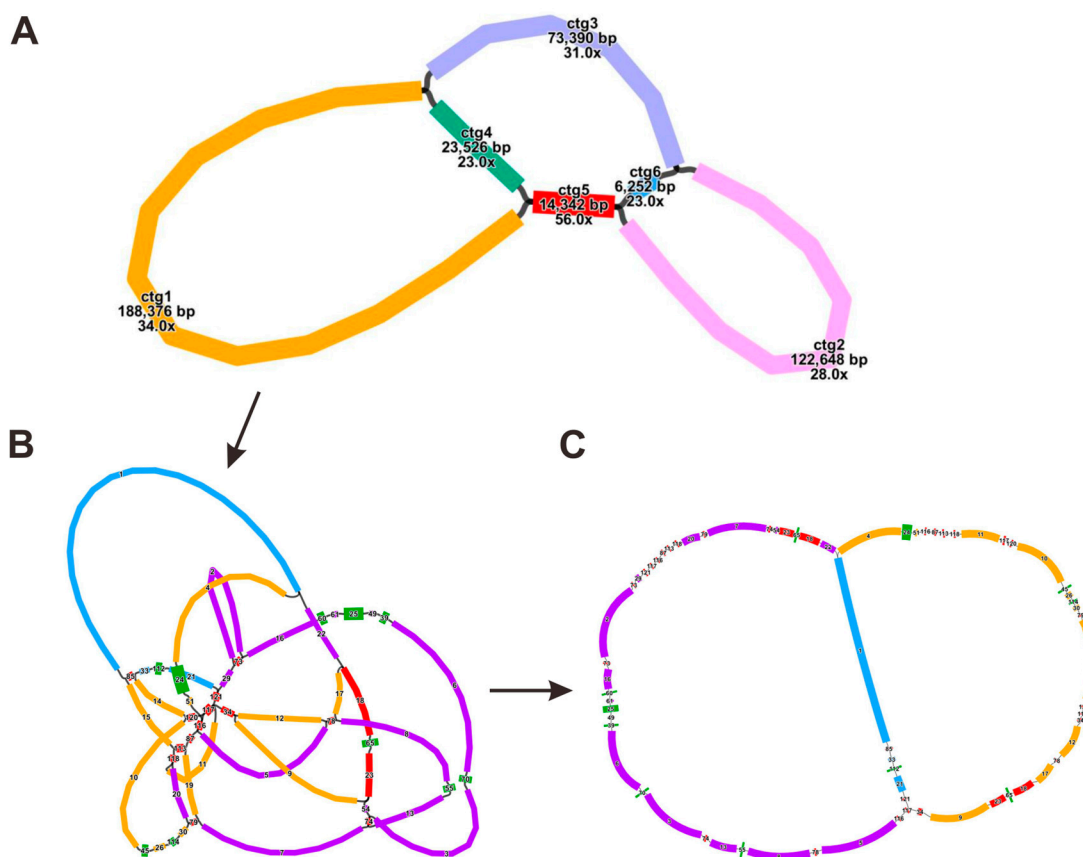


Figure 1. Schematic structure of the mitogenome of *F. qinlingensis* determined using the Bandage software. (A) Draft of the mitogenome assembly with six branch contigs. (B) Multi-branched mitogenome with overlapping nodes colored purple, blue, and yellow. Repetitive sequences are colored red. Green regions indicate the DNA sequences transferred from the plastome. (C) Simplified mitogenome of three overlapping linear molecules (M1, M2, and M3), supported by the PacBio HiFi long-read sequencing data.

Table 1. Analyses of various repetitive nodes based on PacBio HiFi sequencing.

Molecule	Type	Path
M1	linear	117-116-5-78-8-55-13-74-3-70-6-39-49-25-61-60-16-73-2-73-29-121-117-116-87-113-118-20-79-7-74-54-23-65-18-22
M2	linear	4-24-51-116-87-113-118-11-117-120-10-45-26-114-30-79-19-113-15-85-14-120-117-34-12-78-17-18-65-23-9-34
M3	linear	1-85-33-112-21-121

3.2. Mitogenome Annotation of *F. qinlingensis*

The annotated mitogenome revealed that a total of 35 unique protein-encoding genes (PCGs) belonging to 11 significant groups were anchored in the mitogenome of three linear molecules, M1, M2, and M3, of *F. qinlingensis* (Table 2 and Figure 2). Among them,

24 PCGs were classified as endogenous core structural genes, and 11 PCGs were classified as noncore structural genes, including three large ribosomal subunits (*rpl2*, -5, and -16) and eight small ribosomal subunit genes (*rps1*, -3, -4, -7, -12, -13, -14, and -19). The mitochondrial structural PCGs comprised five ATP synthase genes (*atp1*, -4, -6, -8, and -9), nine NADH dehydrogenase genes (*nad1*, -2, -3, -4, *nad4L*, *nad5*, -6, -7, and -9), four ubiquinol-cytochrome c reductase genes (*ccmB*, *ccmC*, *ccmFc*, and *ccmFn*), three cytochrome c oxidase genes (*cox1*, -2, and -3), one membrane transporter gene (*mttB*), one cytochrome b gene (*cob*), and one maturase gene (*matR*). In addition, three single-copy rRNA genes (*rrn5*, -18, and -26) and sixteen tRNA genes, including four two-copy genes (*trnM*-CAU, *trnP*-UGG, *trnR*-ACG, and *trnS*-GCU), were identified as non-PCGs.

Table 2. List of gene annotations in the mitogenome of *F. qinlingensis*.

Gene Group	Gene Name
ATP synthase	<i>atp1</i> (×2*), <i>atp4</i> , <i>atp6</i> , <i>atp8</i> , <i>atp9</i>
NADH dehydrogenase	<i>nad1</i> , <i>nad2</i> , <i>nad3</i> (×2), <i>nad4</i> , <i>nad4L</i> , <i>nad5</i> , <i>nad6</i> , <i>nad7</i> , <i>nad9</i>
Cytochrome b reductase	<i>cob</i>
Ubiquinol cytochrome c reductase	<i>ccmB</i> , <i>ccmC</i> , <i>ccmFC</i> , <i>ccmFN</i>
Cytochrome c oxidase	<i>cox1</i> , <i>cox2</i> , <i>cox3</i>
Maturase	<i>matR</i>
Membrane transport protein	<i>mttB</i>
Ribosomal large subunits	<i>rpl2</i> , <i>rpl5</i> (×2), <i>rpl16</i>
Ribosomal small subunits	<i>rps1</i> , <i>rps3</i> , <i>rps4</i> , <i>rps7</i> , <i>rps12</i> , <i>rps13</i> , <i>rps14</i> (×2), <i>rps19</i>
Ribosome RNA	<i>rrn5</i> , <i>rrn18</i> , <i>rrn26</i> <i>trnC</i> -GCA, <i>trnD</i> -GUC, <i>trnE</i> -UUC, <i>trnF</i> -GAA, <i>trnH</i> -GUG, <i>trnK</i> -UUU, <i>trnM</i> -CAU (×2), <i>trnN</i> -GUU, <i>trnP</i> -UGG (×2), <i>trnQ</i> -UUG, <i>trnR</i> -ACG (×2), <i>trnS</i> -GCU (×2), <i>trnS</i> -UGA, <i>trnT</i> -UGU, <i>trnW</i> -CCA, <i>trnY</i> -GUA

* The number represents the gene's copy number.

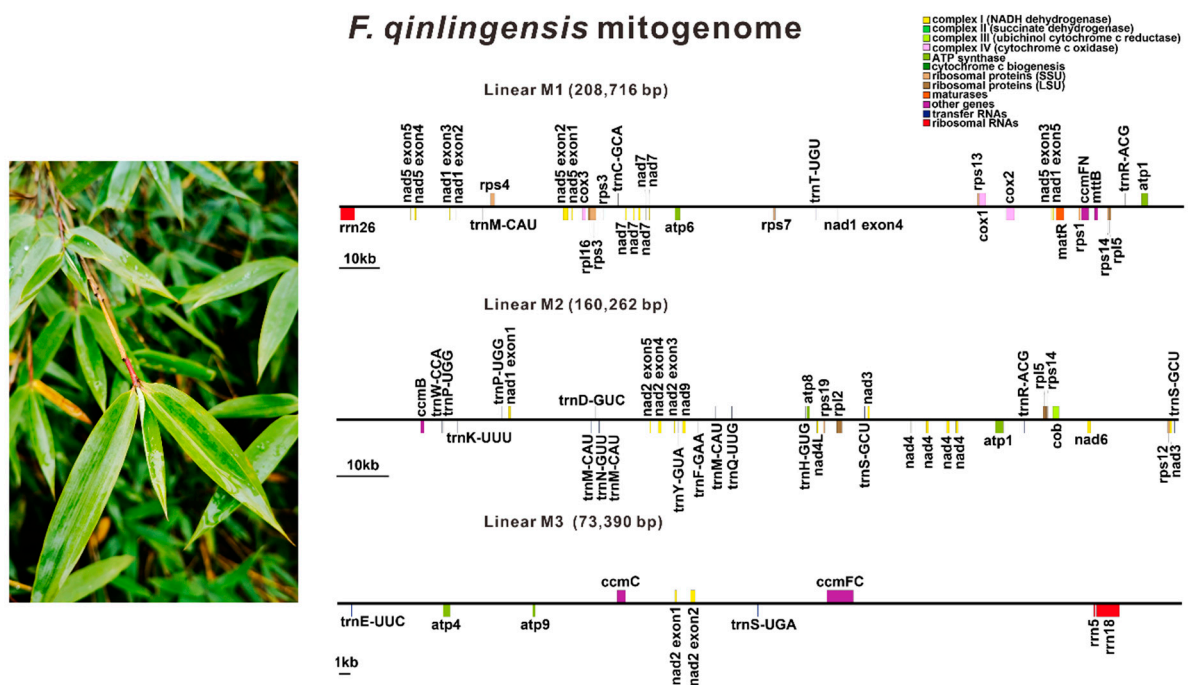


Figure 2. Schematic map of three linearized mitogenomes and gene annotations in *F. qinlingensis*. Different annotated gene families are shown above/below the lines in three linear molecules: M1, M2, and M3.

3.3. Detection of Codon Usage Preference in PCGs

The codon usage preference among all 35 PCGs was deduced using the PhyloSuite and Mega software based on the relative synonymous codon usage (RSCU) value, twenty amino acids, and one terminal codon. The results showed 29 codons (e.g., AGA, CAA, and GGA) that exhibited RSCU values greater than 1 (Figure 3 and Table S5). Interestingly, alanine (Ala) for GCU and glutamine (Gln) for CAA had the most significant codon usage bias (RSCU = 1.55), followed by histidine (His), which showed significant codon usage for CAU (RSCU = 1.54). In contrast, the glycine (Gly) and threonine (Thr) had relatively high RSCU values (1.43) for GGA and ACU, respectively, indicating a strong preference for codon usage. Codon usage bias was compatible with the identified tRNA copy numbers (Table 2).

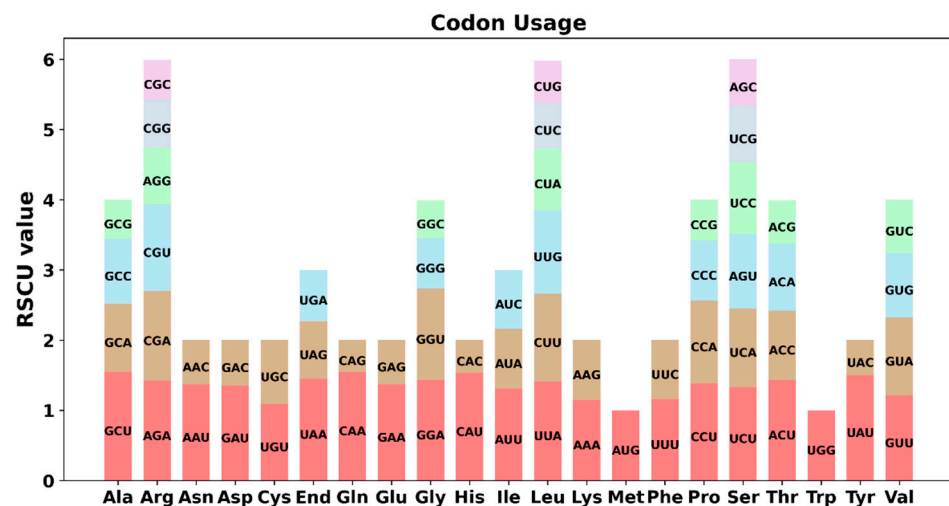


Figure 3. Codon usage preference in 35 PCGs based on the RSCU. X-axis indicates the codon families for amino acids. Y-axis represents the RSCU value. RSCU, relative synonymous codon usage.

3.4. Analyses of Various Types of Repetitive Sequences

Many long repetitive sequences, including tandem and dispersed repeats, which determine structural variations, are generated in plant mitogenomes through genome recombination [44]. Simple sequence repeats (SSRs) are uncommon tandem repeats (7–200 bp) less than 6 bp in length. The cyclic maps illustrated the distributions and links of the repetitive sequences, including palindromic and forward repeats, tandem repeats, and SSRs, across the three linear mitogenome molecules (Figure 4). Approximately 51, 28, and 14 SSRs were identified primarily in monomeric and dimeric repetitive forms, accounting for 41.18%, 42.86%, and 50.00% of the linear molecules, M1, M2, and M3, respectively (Table S6). A total of 42 tandem repeats (24 in M1, 16 in M2, and 2 in M3) were observed, ranging in size from 11 to 41 bp. In addition, dispersed repeats frequently occurred in the particular forms of forward repeats/palindromic repeats detected, with 71 (46/25) in M1, 72 (34/38) in M2, and 10 (6/4) in M3 (Tables S7 and S8).

The complete plastome of *F. qinlingensis* was initially deciphered, exhibiting a length of 139,776 bp and a GC content of 38.88% (Figure 5A). BWA BLAST revealed forty-four fragments (30,943 bp) of MTPTs with significant homology to those in the plastome, accounting for 6.99% of the entire mitogenome. A total of eight MTPTs were identified to have an extended sequence length of more than 1 kb, including one that displayed the mostly extended length (5131 bp) in M1, containing two partial PCGs (*rpoB* and *C2*) and one intact *rpoC1*, compared with the others, which ranged from 33 to 4116 bp (Figure 5B and Table S9). In addition, many long-read sequences spanning the MTPTs were blasted, which may support conformation and DNA recombination (Tables S2 and S3). The annotation of the MTPTs revealed the presence of 20 full-length genes, including 10 PCGs (*atpE*, *ndhI*, *ndhJ*, *petB*, *psaB*, *psbH*, *psbM*, *psbN*, *rpoC1*, and *rps4*) and ten tRNAs (*trnF-GAA*,

trnC-GCA, trnH-GUG, trnM-CAU, trnN-GUU, trnP-GGG, trnR-ACG, trnW-CCA, trnV-UAC, and trnS-GGA).

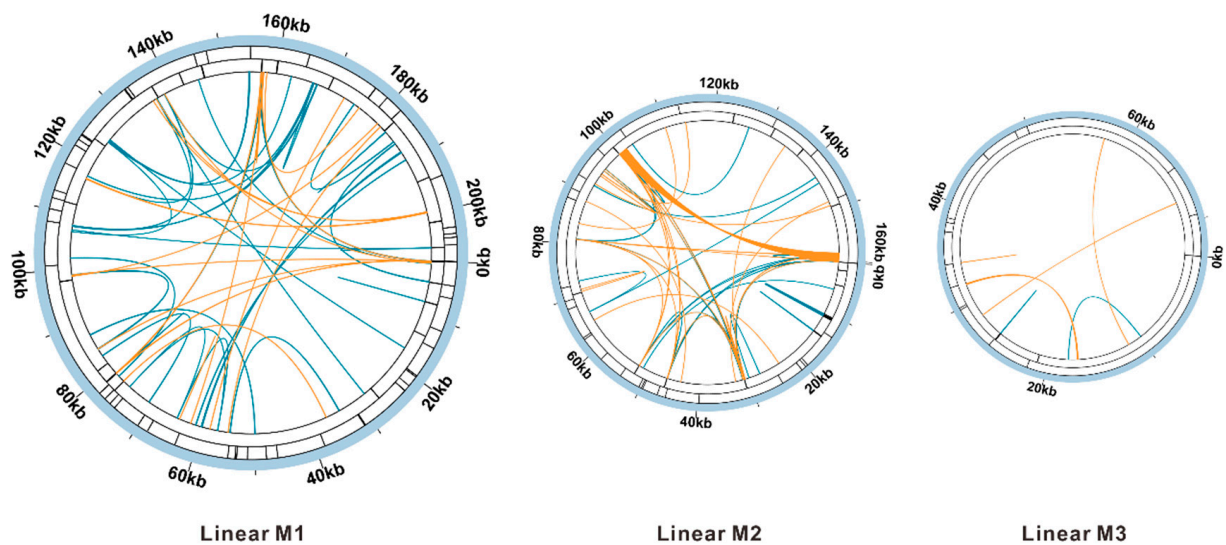


Figure 4. Repetitive sequences identified in the three molecules, M1, M2, and M3, of *F. qinlingensis*. Cyclic maps illustrate the distributions of three types of linked repetitive sequences, including dispersed repeats (palindromic repeats in orange and forward repeats in blue), tandem repeats (black lines in the second ring), and SSRs (black lines in the outer ring).

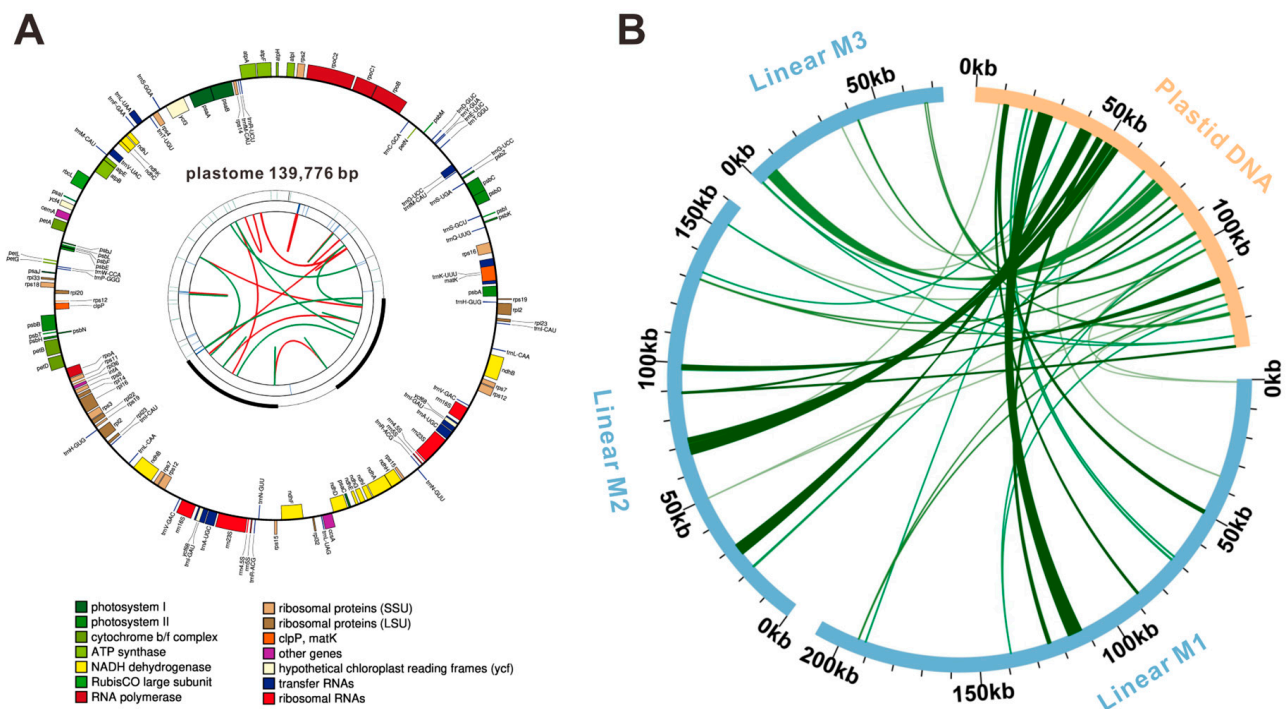


Figure 5. Plastome and plastid DNA migration in the mitogenome. (A) Assembled circular plastome, showing the sequence length and annotated genes. (B) MTPTs identified in the *F. qinlingensis* mitogenome. Green ribbons represent homologous MTPTs transferred between two organelles. MTPT, mitochondrial plastid DNA.

3.5. Prediction of RNA-Editing Sites and Experimental Evaluation

Modification of the RNA sequence, namely RNA-editing, commonly occurs at specific sites and creates products that differ from DNA [45,46]. The RNA-editing sites of all annotated PCGs from the *F. qinlingensis* mitogenome were predicted using BEDTools.

Under these criteria (cutoff = 0.2), a total of 482 potential RNA-editing sites with cytidine (C) to thymine (T)/uridine (U) transformation were characterized (Figure 6A and Table S10). The highest frequency was found for *ccmFn* with 38 editing sites, followed by *ccmC* with 36. The *rpl2* and *rps7* genes had single RNA-editing sites, whereas *rps14* displayed no editing sites. The accuracy of the identification of four critical PCGs (*atp9*, *cox2*, *nad1*, and *nad7*) with start, stop, and sense codons in the mitogenome was validated by the retention of 71 putative RNA-editing sites. Sanger sequencing of the PCR amplified products was conducted using synthesized complementary DNA (cDNA) and DNA as templates. The sequence length of the PCR products covered 31 RNA-editing sites (e.g., *atp9-191*, *cox2-353*, *cox2-608*, *nad1-216*, and *nad7-224*) that were experimentally evaluated (Figure 6B and Table S11). Based on the sequencing data, the changes in bases between the DNA and cDNA PCR-amplified sequences successfully verified 27 RNA-editing sites (A-T), accounting for 87.09% consistency in the prediction (Figure S3).

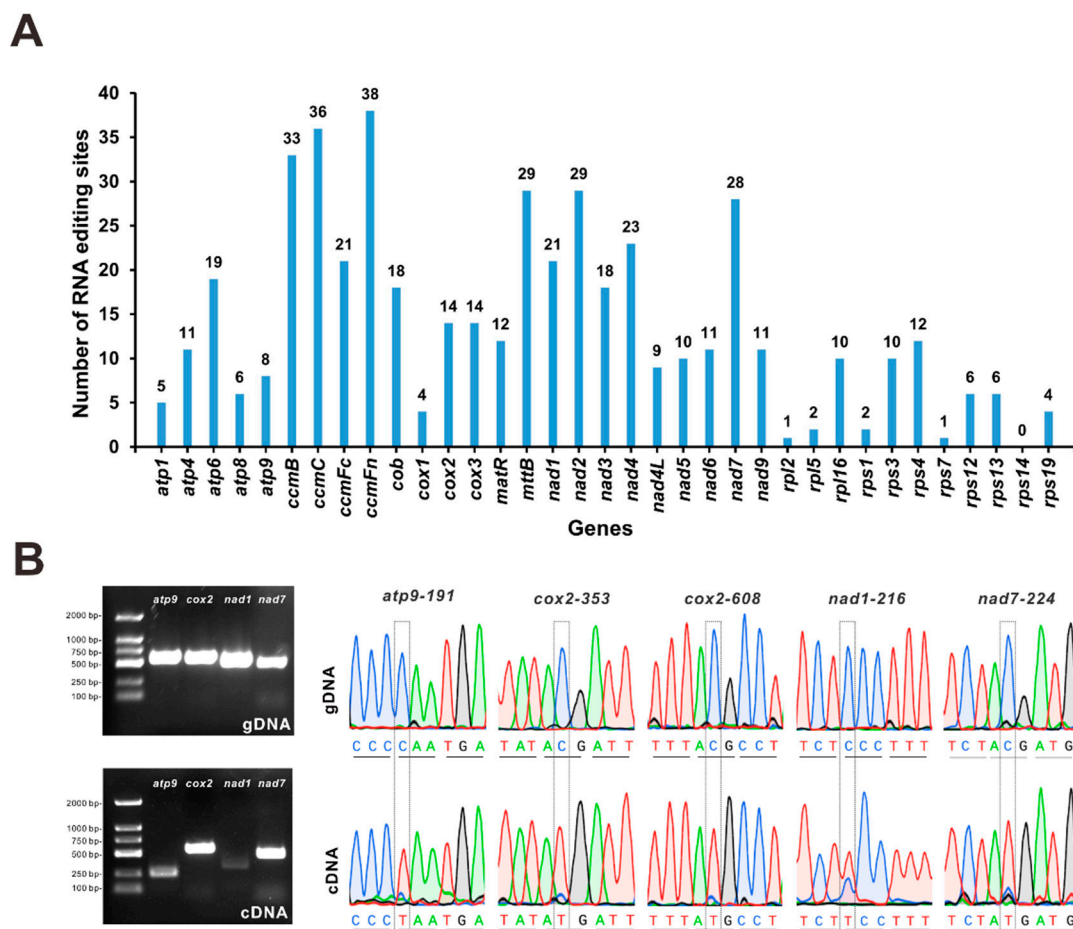


Figure 6. Prediction of RNA-editing sites in 35 PCGs and the experimental evaluation. (A) PCR amplification was conducted using DNA and cDNA as templates. (B) Experimental confirmation of the RNA-editing sites in selected PCGs (*atp9-191*, *cox2-353*, *-608*, *nad1-216*, and *nad7-224*), showing the exemplified C to T changes (dotted line framed) via Sanger sequencing.

3.6. Sequence Collinearity and Phylogenetic Evolution

Multiple collinear plots revealed the synteny patterns between the full-length mitogenome sequences of seven plant species in the subfamilies of Pooideae and Bambusoideae (Figure 7A and Table S12). The identified blank regions were considered individual blocks within a particular species. Some short homologous blocks were detected between *F. qinlingensis* and other genetically related species, indicating non-conserved relationships owing to mitogenome rearrangement and reorganization [47]. Subsequently, phylogenetic analyses were performed using the available mitogenomes from six related subfamilies

(Pooideae, Bambusoideae, Oryzoideae, Panicoideae, Chloridoideae, and Puelieae), comprising 21 plant species. *Acacia* (*A. ligulata* A. Cunn. ex Benth.) was used as an outgroup (Figure 7B and Table S12). Approximately eighteen conserved PCGs shared patterns among all examined species, including seven *nads* (*nad1*, -2, -3, -4, -5, -6, and -7), three *atps* (*atp4* and *atp6*), three *ccms* (*ccmC*, -Fc, and -B), three *coxs* (*cox1*, -2 and -3), *rpss* (*rps3* and *rps4*), and the *cob* and *rpl16* genes. Species clustered into the same family were classified in the phylogenetic topology, coinciding with the latest classification [16,48]. Based on the unrooted phylogenetic trees, *F. qinlingensis* was closely related to *Bambusa* (*B. oldhamii* Munro.) in the Bambusoideae (Poaceae) subclade.

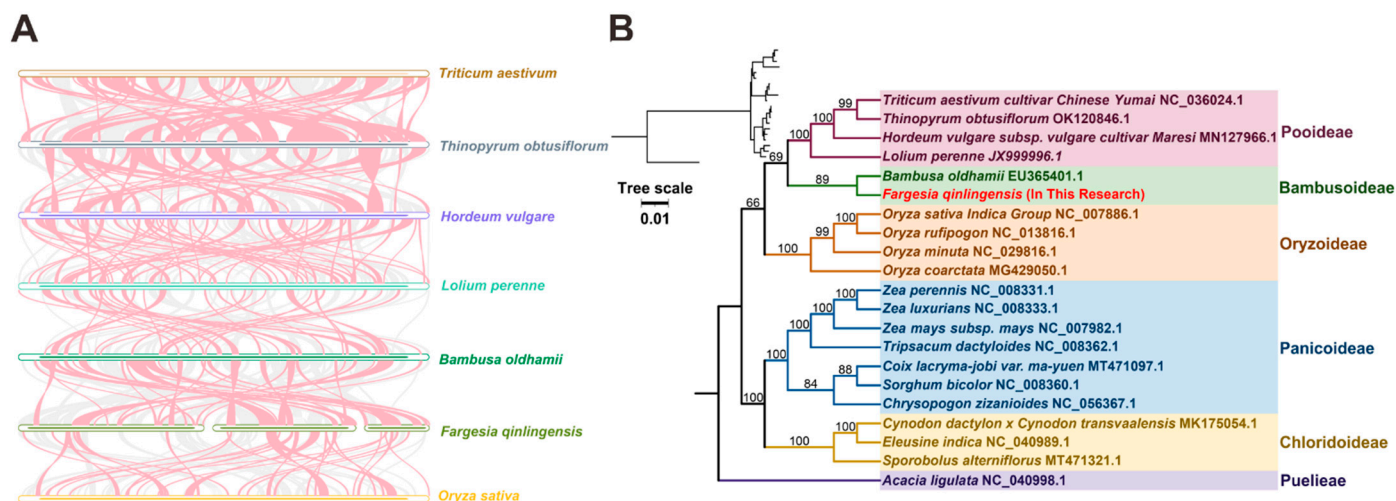


Figure 7. Collinearity and evolutionary relationships between *F. qinlingensis* and other plants. (A) Synteny analyses of seven mitogenomes within Pooideae and Bambusoideae. Pink-curved ribbons represent DNA inversion regions, and gray-curved ribbons indicate sites with high homology. Collinear blocks with sequence lengths < 0.5 kb were not retained. (B) Phylogenetic relationships between *F. qinlingensis* and 28 genetically related species shown using full-length mitogenome sequences. This unrooted tree was constructed using the neighbor-joining method.

4. Discussion

Technological advances and innovations in genome sequencing and assembly have led to a meteoric rise in published organelle genomes, highlighting the significance of diverse evolutionary trajectories [49]. High-throughput sequencing techniques have revolutionized our understanding of genomes and transcriptomes, enabling the cost-effective and efficient deciphering of high-quality mitogenome structures [50]. The number of reported complete mitogenomes in plants is continually increasing, and these mitogenomes are being employed in studies related to phylogenetic evolution, biological conservation, and other taxonomic areas. Many *Fargesia* species endemically grow in subalpine mountain forests, of which *F. qinlingensis* is a staple bamboo and critical shelter for the wild giant panda [51]. The mitogenomes of diverse plant families have been investigated to obtain phylogenetic information. Nevertheless, the molecular functions of mitochondrial genes involved in stress acclimation and the role of mitochondrial DNA in evolutionary relationships and species-level classification in bamboo remain largely unknown. Despite its ecological and economic significance, the molecular basis of the *F. qinlingensis* species remains unexplored and overlooked due to the molecular complexity of its polyphyletic origin and evolutionary diversity [52].

The elusive mitochondrial signal has now been postulated to be a central hub involved in intracellular interactions and the homeostasis of ROS in multiple organisms [53]. Mitochondrial genes/proteins are targets of extensive posttranscriptional and posttranslational modifications; however, their functional and physiological significance remains unclear [54]. Understanding the mitogenome together with its structural genes is essential

for elucidating its replication, biological function, inheritance, and phylogenetic trajectories [7]. In this study, we implemented a hybrid strategy based on Illumina short-read and PacBio HiFi long-read sequencing to decipher the mitogenome conformation and structure of *F. qinlingensis*. The complete mitogenome showed a total length of 442,368 bp with a GC content of 44.05% and 35 annotated mitochondrial PCGs, suggesting moderate conservation among bamboo species [23]. Our work demonstrated that the high-resolution mitogenome in the *Fargesia* genus is not a single linear structure but rather a dynamic, complex, and multi-branched conformation composed of a mixture of three linear molecules (Figures 1 and 2). In a few reports, mitogenome structures are linear or linear–circular combinations of DNA molecules, as identified in rice (*Oryza sativa* L.) and spearmint (*Mentha spicata* L.) [49,55]. Some recent studies have revealed that resolved plant mitogenomes comprise multi-circular molecules/chromosomes or combined structures [56–58]. Due to ongoing genome replication, frequent homologous DNA rearrangements, gene loss, or migration from the plastome and nuclear genome, the mitogenome conformation and size are variable among various plant lineages [47]. Therefore, more marked mitogenomic architecture and length variations commonly occur in plants than in animals due to the high number of sequence repeats and significant complexity [50]. Extensive genomic recombination and sequence rearrangements were identified in the mitogenome of *F. qinlingensis* and its genetically related species, while the 18 PCGs showed highly conserved patterns. Deciphering the mitogenome of *F. qinlingensis* will aid in understanding its evolutionary patterns, facilitating endeavors to explore the molecular mechanisms underlying climate adaptation and providing a theoretical basis for improving the biological conservation and growth performance of the Bambusoideae.

Significant genome variation and diversity in mitochondrial structural genes and intron contents occurred across eukaryotes, indicating massive convergent evolution [59]. Plant mitogenomes exhibit fewer mutations and more DNA rearrangements than animal mitogenomes [60]. The prolonged endosymbiotic origin of mitochondria results in the loss of some original DNA, with only critical functions remaining owing to DNA migration between different organelles [61]. The conserved patterns of plant mitogenomes (e.g., compactness, high copy number, and frequent rearrangements) reflect a complex evolutionary history and ongoing ecological adaptation to critical environmental cues [62]. Therefore, understanding mitogenome structural variation and diversity provides a basis for unveiling plant functional significance and evolutionary patterns.

In evolution, the mitogenome is considered an entity that has undergone dynamic changes, displaying substantial variation in structure and size among various plants [56]. Exogenous sequence insertions and repeats in plant mitogenomes often lead to gene imbalances, multiple copy numbers, and DNA rearrangements, resulting in multi-branched conformations [8,63]. In our work, the comparative analysis revealed a more conserved mitogenome size and gene content in *F. qinlingensis*, albeit the prolonged length in the linear mitogenome of *Cinnamomum camphora* has been observed [64]. Among angiosperms, forty-one standard PCGs commonly occur in the ancestor's mitogenome [65]. In the mitogenome of *F. qinlingensis*, thirty-five structural genes were annotated (twenty-four core and eleven noncore PCGs), reflecting a common phenomenon of gene loss, possibly due to DNA migration into the nucleus during long-term genome evolution. As the primary carriers in nature, triplet codons maintain the precise translation and transmission of genetic information, playing a crucial role in biology and genetic variation [66]. Principally, except for the start codon (methionine) and tryptophan, the remaining eighteen typical amino acids are composed of natural proteins corresponding to two to six synonymous codons [67]. The selection of synonymous codons does not alter amino acids, which benefits translation accuracy and affects the expression levels of particular proteins [68]. Approximately twenty-nine codons showed significance, pointing out a constant evolution trend of base composition, which fits well with a recent report on codon usage analyses in *Agrostis stolonifera* L. [69]. Our results support the use of heterologous genes for codon optimization and enhancing mitochondrial protein expression in *F. qinlingensis*.

As mitogenomes are irreplaceable in promoting intermolecular recombination mechanisms, many reports have highlighted the intrinsic value of these repetitive sequences [50]. These repetitive sequences are paramount in determining the mitogenome shape and profoundly influence mitogenome structure and dynamic function [70]. In the present work, various types of sequence repeats (e.g., SSRs, long tandem repeats, and dispersed repeats) in the mitogenome of *F. qinlingensis* were extensively investigated. The results suggested that intermolecular DNA recombination may have altered the dynamic conformation and size of the mitogenome during genome evolution. All eight pairs of long repetitive sequences had long reads that supported the recombination conformation. Long reads provide a detailed review of mitogenome variants, so only long reads were used for structure validation [71]. For the most extended repetitive sequences, 20.519 kb of MPTs, similar to the plastid inverted repeat (IR) region, usually accounted for a large proportion of the mitochondrial DNA rearrangement (Table S9). Experimental PCR evaluation can be applied to the boundaries of the longer repeat segments. Many MPTs initially identified in the mitogenome have been lost during genetic evolution because of functional traits and stress adaptation [9]. As the plastid DNA transfer to the mitogenome occurred during the genome evolution, the tRNA gene transfer was considered a joint event in angiosperm lineages [1].

Nevertheless, due to the contraction of IRs and intriguing sequence insertion, opposite directions of DNA migration from the mitogenome to the plastome have been characterized in bamboos within two eudicot lineages, suggesting the prevalence of coexisting and intracellular horizontal DNA transfer between these two plant organelles [72]. The succinate dehydrogenase gene (*sdh2*) was reported to have been lost during early genome evolution, indicating that several structural genes (e.g., *rps9*, *-11*, and *-16*) were not conserved in various plant kingdoms [73]. A similar phenomenon was observed in the rice mitogenome, lacking the *rps12*, *sdh3*, and *sdh4* genes. However, *rps2* shares conserved features with monocot lineages, suggesting that natural selection and environmental pressures influence the mitogenome architecture [55]. In the mitogenome of *F. qinlingensis*, a total of 44 MPTs were recognized, indicating horizontal DNA transfer and evolutionary diversity. This included ten PCGs and ten tRNA genes, accounting for 6.99% of the total DNA migration from the plastome, which is consistent with previous findings [74].

Following the posttranscriptional mechanisms between the plastome and mitogenome, RNA-editing is an enigmatic reaction at the RNA level that sustains fine-tuned protein folding and biological functions in flowering plants [46]. The predominant type of RNA-editing is the conversion from C to U, occasionally accompanied by U–C conversions [45]. Changes in the dosage of DNA/RNA base conversion may result in the rewriting of the RNA sequence, thus impacting translation, protein folding, and organelle interactions [75]. Recent innovations in high-throughput sequencing techniques have significantly promoted the release of numerous complete genomes and transcriptomes, thus providing novel insights into RNA-editing across various plant species [45]. Previous reports revealed that RNA-editing in mitochondrial *atp1* affected ATP production and the elongation of cotton (*Gossypium hirsutum* L.) trichome and fibers [76]. A total of 441 RNA-editing sites were deduced to span 36 PCGs in the *Arabidopsis* mitogenome [75]. In addition, approximately 491 RNA-editing sites were identified in 34 PCGs from a model monocot of the rice mitogenome [55]. Recently, the mitogenome of a halophyte species (*S. glauca*) revealed 216 RNA-editing sites within 26 PCGs [77]. The increased numbers of RNA-editing sites in *nad4*, a central subunit of the mitochondrial respiratory chain complex I, may reflect its potential role in regulating cellular metabolism, including ATP synthesis and oxidative phosphorylation [78]. Notably, the genetic association of COX-related genes in dysfunctional mitochondria with Alzheimer's disease has been shown to have functional relevance in plants [79,80]. RNA-editing sites predicted among the 31 PCGs in the mitogenome of *F. qinlingensis* suggested increased overall conservation of amino acids associated with the physicochemical properties and functions of the specific protein. Only one RNA-editing site was identified in *atp8*, *rps7*, and *rps13*, indicating that sequence variation and conservation

were retained during mitogenome evolution. RNA-editing events were experimentally confirmed using Sanger sequencing and comparing the PCR-amplified products.

Furthermore, the collinear analyses revealed that *F. qinlingensis* had relatively good synteny blocks but lacked conservative relationships with other species within the two subfamilies (Pooideae and Bambusoideae). This finding indicates that they underwent extensive DNA rearrangement and migration during genome evolution and natural selection. In addition, the phylogenies were determined using multiple mitogenome alignments among four representative orders comprising *F. qinlingensis* and 20 other species. The unrooted phylogenetic tree infers a well-defined taxonomic relationship between different subfamilies. Notably, *F. qinlingensis* appeared to have evolved more closely to *B. oldhamii*. A recent study revealed the taxonomical difficulties in species identification using complete plastome and nuclear ribosomal DNA sequences, highlighting the long generation time and complex evolutionary history of the *Fargesia* genus [15,16]. Our phylogenetic work revealed the potential benefits of studying the *Fargesia* mitogenome.

5. Conclusions

Integrated Illumina and PacBio HiFi hybrid sequencing assays allowed us to obtain the first high-quality mitogenome of *F. qinlingensis*, revealing a multi-branched structure of three linearized molecules (M1, M2, and M3). The complete mitogenome was assembled and analyzed to capture the spectrum of annotated gene isoforms, providing intensive insights into the complex architecture and rearrangement activities of the *F. qinlingensis* mitogenome. Unraveling the mitogenome of *Fargesia* has molecular implications linked with ecological and biological benefits, as well as efforts to develop strategies for climate resilience and biological conservation associated with mitochondrial traits in mountain forests. Nevertheless, the resulting unrooted trees reveal a significant deficiency in bamboo mitogenome pools; thus, strategies to promote the flourishing of *Fargesia* within bamboo clades are urgently needed. Our work lays the foundation for future research, unveiling the mechanisms underlying genetic evolution, stress adaptation, and sustainability combined with the nuclear genomes and plastomes of the *Fargesia* genus.

Supplementary Materials: The following supporting information can be downloaded at <https://www.mdpi.com/article/10.3390/f15071267/s1>. Figure S1: Sequencing depth of coverage based on Illumina short reads (left panel) and PacBio HiFi long reads (right panel); Figure S2: Mitogenome conformation changes from different path combinations; Figure S3: Validations of the RNA-editing sites in four selected PCGs using Sanger sequencing; Table S1: Qualimap analyses of mitogenome assembly in *F. qinlingensis*; Table S2: Potential paths and number of long reads. Table S3: Collection of long reads obtained from BLASTn results supporting different paths; Table S4: Basic information on the *F. qinlingensis* mitogenome; Table S5: Relative synonymous codon usage in the *F. qinlingensis* mitogenome; Table S6: SSRs in the mitogenome of M1, M2, and M3; Table S7: Tandem repeat sequences in the mitogenome of M1, M2, and M3; Table S8: Dispersed repeat sequences in the mitogenome of M1, M2, and M3; Table S9: Homologous migrated DNA fragments in the *F. qinlingensis* mitogenome; Table S10: RNA-editing prediction in the *F. qinlingensis* mitogenome; Table S11: Primer sequences used for evaluating RNA-editing sites; Table S12: NCBI accession numbers of plant mitogenomes.

Author Contributions: H.W., X.L. and K.Q.: conceptualization, investigation, formal analysis, and writing—original draft. L.Y. (Lele Yang) and L.Y. (Lijun Yong): resources, formal analysis, data curation, and software. T.S. and M.H.: conceptualization, supervision, project administration, and writing—review and editing. F.C.: funding acquisition, supervision, and writing—review and editing. All authors have read and agreed to the published version of the manuscript.

Funding: This research was funded by the National Key Technology Research and Development Program (2021YFD2200503), the Postgraduate Research and Practice Innovation Program of Jiangsu Province (SJCX22_0329), and the National Natural Science Foundation of China (31870589), and the Natural Science Foundation of Jiangsu Province (BK20170921).

Data Availability Statement: In this study, the assembled mitogenome sequences of the *F. qinlingensis* were submitted to the GenBank database with the following accession IDs: OP324798, M1, OP324799, M2, and OP324800, M3. The assembled plastome of *F. qinlingensis* was deposited in the GenBank database with the following accession ID: MZ905454. The following SRA numbers are available for the raw data in the GenBank database with the following SRA IDs: SRR27909850, Illumina short reads, and SRR29094227, PacBio HiFi long reads.

Acknowledgments: The authors thank all funding agencies for supporting this work. We thank the Co-Innovation Center for Sustainable Forestry in Southern China, the State Key Laboratory of Tree Genetics and Breeding, and the Priority Academic Program Development of Jiangsu Higher Education Institutions for using instruments.

Conflicts of Interest: The authors declare no conflicts of interest.

References

1. Turmel, M.; Lopes dos Santos, A.; Otis, C.; Sergerie, R.; Lemieux, C. Tracing the Evolution of the Plastome and Mitogenome in the Chloropicophyceae Uncovered Convergent tRNA Gene Losses and a Variant Plastid Genetic Code. *Genome Biol. Evol.* **2019**, *11*, 1275–1292. [[CrossRef](#)]
2. Kummer, E.; Ban, N. Mechanisms and regulation of protein synthesis in mitochondria. *Nat. Rev. Mol. Cell Biol.* **2021**, *22*, 307–325. [[CrossRef](#)] [[PubMed](#)]
3. Zheng, W.; Chai, P.; Zhu, J.; Zhang, K. High-resolution in situ structures of mammalian respiratory supercomplexes. *Nature* **2024**, *631*, 232–239. [[CrossRef](#)] [[PubMed](#)]
4. Møller, I.M.; Rasmusson, A.G.; Van Aken, O. Plant mitochondria—Past, present and future. *Plant J.* **2021**, *108*, 912–959. [[CrossRef](#)] [[PubMed](#)]
5. Ghifari, A.S.; Saha, S.; Murcha, M.W. The biogenesis and regulation of the plant oxidative phosphorylation system. *Plant Physiol.* **2023**, *192*, 728–747. [[CrossRef](#)] [[PubMed](#)]
6. Munasinghe, M.; Ågren, J.A. When and why are mitochondria paternally inherited? *Curr. Opin. Genet. Dev.* **2023**, *80*, 102053. [[CrossRef](#)] [[PubMed](#)]
7. Kozik, A.; Rowan, B.A.; Lavelle, D.; Berke, L.; Eric Schranz, M.; Michelmore, R.W.; Christensen, A.C. The alternative reality of plant mitochondrial DNA: One ring does not rule them all. *PLoS Genet.* **2019**, *15*, e1008373. [[CrossRef](#)] [[PubMed](#)]
8. Wu, Z.; Liao, X.; Zhang, X.; Tembrock, L.R.; Broz, A. Genomic architectural variation of plant mitochondria—A review of multichromosomal structuring. *J. Syst. Evol.* **2022**, *60*, 160–168. [[CrossRef](#)]
9. Lei, B.; Li, S.; Liu, G.; Chen, Z.; Su, A.; Li, P.; Li, Z.; Hua, J. Evolution of mitochondrial gene content: Loss of genes, tRNAs and introns between *Gossypium harknessii* and other plants. *Plant Syst. Evol.* **2013**, *299*, 1889–1897. [[CrossRef](#)]
10. Grewe, F.; Viehoveer, P.; Weisshaar, B.; Knoop, V. A trans-splicing group I intron and tRNA-hyperediting in the mitochondrial genome of the lycophyte *Isoetes engelmannii*. *Nucleic Acids Res.* **2009**, *37*, 5093–5104. [[CrossRef](#)]
11. Tong, W.; Kim, T.-S.; Park, Y.-J. Rice Chloroplast Genome Variation Architecture and Phylogenetic Dissection in Diverse *Oryza* Species Assessed by Whole-Genome Resequencing. *Rice* **2016**, *9*, 57. [[CrossRef](#)] [[PubMed](#)]
12. Soreng, R.J.; Peterson, P.M.; Zuloaga, F.O.; Romaschenko, K.; Clark, L.G.; Teisher, J.K.; Gillespie, L.J.; Barberá, P.; Welker, C.A.D.; Kellogg, E.A.; et al. A worldwide phylogenetic classification of the Poaceae (Gramineae) III: An update. *J. Syst. Evol.* **2022**, *60*, 476–521. [[CrossRef](#)]
13. Guo, Z.-H.; Ma, P.-F.; Yang, G.-Q.; Hu, J.-Y.; Liu, Y.-L.; Xia, E.-H.; Zhong, M.-C.; Zhao, L.; Sun, G.-L.; Xu, Y.-X.; et al. Genome Sequences Provide Insights into the Reticulate Origin and Unique Traits of Woody Bamboos. *Mol. Plant* **2019**, *12*, 1353–1365. [[CrossRef](#)] [[PubMed](#)]
14. Ruiz-Sanchez, E.; Tyrrell, C.D.; Londoño, X.; Oliveira, R.P.; Clark, L.G. Diversity, distribution, and classification of neotropical woody bamboos (Poaceae: Bambusoideae) in the 21st century. *Bot. Sci.* **2021**, *99*, 198–228. [[CrossRef](#)]
15. Lv, S.-Y.; Ye, X.-Y.; Li, Z.-H.; Ma, P.-F.; Li, D.-Z. Testing complete plastomes and nuclear ribosomal DNA sequences for species identification in a taxonomically difficult bamboo genus *Fargesia*. *Plant Divers.* **2023**, *45*, 147–155. [[CrossRef](#)] [[PubMed](#)]
16. Zhou, Y.; Zhang, Y.-Q.; Xing, X.-C.; Zhang, J.-Q.; Ren, Y. Straight From the Plastome: Molecular Phylogeny and Morphological Evolution of *Fargesia* (Bambusoideae: Poaceae). *Front. Plant Sci.* **2019**, *10*, 981. [[CrossRef](#)] [[PubMed](#)]
17. Wang, L.; Yuan, S.; Nie, Y.; Zhao, J.; Cao, X.; Dai, Y.; Zhang, Z.; Wei, F. Dietary flavonoids and the altitudinal preference of wild giant pandas in Foping National Nature Reserve, China. *Glob. Ecol. Conserv.* **2020**, *22*, e00981. [[CrossRef](#)]
18. Du, X.C.; Ren, Y.; Di Dang, G.; Lundholm, J. Distribution and plant community associations of the understory bamboo *Fargesia qinlingensis* in the Foping National Nature Reserve, China. *Ann. For. Sci.* **2011**, *68*, 1197–1206. [[CrossRef](#)]
19. Wang, W.; Franklin, S.B.; Lu, Z.; Rude, B.J. Delayed Flowering in Bamboo: Evidence from *Fargesia qinlingensis* in the Qinling Mountains of China. *Front. Plant Sci.* **2016**, *7*, 151. [[CrossRef](#)]
20. Ye, X.; Ma, P.; Yang, G.; Guo, C.; Zhang, Y.; Chen, Y.; Guo, Z.; Li, D. Rapid diversification of alpine bamboos associated with the uplift of the Hengduan Mountains. *J. Biogeogr.* **2019**, *46*, 2678–2689. [[CrossRef](#)]
21. Porcher, A.; Kangasjärvi, S. Plant biology: Unlocking mitochondrial stress signals. *Curr. Biol.* **2024**, *34*, R59–R61. [[CrossRef](#)]

22. Guo, S.; Li, Z.; Li, C.; Liu, Y.; Liang, X.; Qin, Y. Assembly and characterization of the complete mitochondrial genome of *Ventilago leiocarpa*. *Plant Cell Rep.* **2024**, *43*, 77. [[CrossRef](#)] [[PubMed](#)]
23. Ma, P.-F.; Guo, Z.-H.; Li, D.-Z. Rapid Sequencing of the Bamboo Mitochondrial Genome Using Illumina Technology and Parallel Episodic Evolution of Organelle Genomes in Grasses. *PLoS ONE* **2012**, *7*, e30297. [[CrossRef](#)] [[PubMed](#)]
24. Arseneau, J.; Steeves, R.; Laflamme, M. Modified low-salt CTAB extraction of high-quality DNA from contaminant-rich tissues. *Mol. Ecol. Resour.* **2017**, *17*, 686–693. [[CrossRef](#)]
25. Jin, J.-J.; Yu, W.-B.; Yang, J.-B.; Song, Y.; DePamphilis, C.W.; Yi, T.-S.; Li, D.-Z. GetOrganelle: A fast and versatile toolkit for accurate de novo assembly of organelle genomes. *Genome Biol.* **2020**, *21*, 241. [[CrossRef](#)]
26. Wick, R.R.; Schultz, M.B.; Zobel, J.; Holt, K.E. Bandage: Interactive visualization of de novo genome assemblies. *Bioinformatics* **2015**, *31*, 3350–3352. [[CrossRef](#)]
27. Li, H.; Durbin, R. Fast and accurate short read alignment with Burrows–Wheeler transform. *Bioinformatics* **2009**, *25*, 1754–1760. [[CrossRef](#)] [[PubMed](#)]
28. Tillich, M.; Lehwark, P.; Pellizzer, T.; Ulbricht-Jones, E.S.; Fischer, A.; Bock, R.; Greiner, S. GeSeq—Versatile and accurate annotation of organelle genomes. *Nucleic Acids Res.* **2017**, *45*, W6–W11. [[CrossRef](#)]
29. Chen, Y.; Ye, W.; Zhang, Y.; Xu, Y. High speed BLASTN: An accelerated MegaBLAST search tool. *Nucleic Acids Res.* **2015**, *43*, 7762–7768. [[CrossRef](#)]
30. Chan, P.P.; Lin, B.Y.; Mak, A.J.; Lowe, T.M. tRNAscan-SE 2.0: Improved detection and functional classification of transfer RNA genes. *Nucleic Acids Res.* **2021**, *49*, 9077–9096. [[CrossRef](#)]
31. Kumar, S.; Stecher, G.; Li, M.; Knyaz, C.; Tamura, K. MEGA X: Molecular Evolutionary Genetics Analysis across Computing Platforms. *Mol. Biol. Evol.* **2018**, *35*, 1547–1549. [[CrossRef](#)] [[PubMed](#)]
32. Zhang, D.; Gao, F.; Jakovlić, I.; Zou, H.; Zhang, J.; Li, W.X.; Wang, G.T. PhyloSuite: An integrated and scalable desktop platform for streamlined molecular sequence data management and evolutionary phylogenetics studies. *Mol. Ecol. Resour.* **2020**, *20*, 348–355. [[CrossRef](#)] [[PubMed](#)]
33. Benson, G. Tandem repeats finder: A program to analyze DNA sequences. *Nucleic Acids Res.* **1999**, *27*, 573–580. [[CrossRef](#)] [[PubMed](#)]
34. Kurtz, S. REPuter: The manifold applications of repeat analysis on a genomic scale. *Nucleic Acids Res.* **2001**, *29*, 4633–4642. [[CrossRef](#)] [[PubMed](#)]
35. Zhang, H.; Meltzer, P.; Davis, S. RCircos: An R package for Circos 2D track plots. *BMC Bioinform.* **2013**, *14*, 244. [[CrossRef](#)] [[PubMed](#)]
36. Shi, L.; Chen, H.; Jiang, M.; Wang, L.; Wu, X.; Huang, L.; Liu, C. CPGAVAS2, an integrated plastome sequence annotator and analyzer. *Nucleic Acids Res.* **2019**, *47*, W65–W73. [[CrossRef](#)] [[PubMed](#)]
37. Chen, C.; Chen, H.; Zhang, Y.; Thomas, H.R.; Frank, M.H.; He, Y.; Xia, R. TBtools: An Integrative Toolkit Developed for Interactive Analyses of Big Biological Data. *Mol. Plant* **2020**, *13*, 1194–1202. [[CrossRef](#)] [[PubMed](#)]
38. Milne, I.; Stephen, G.; Bayer, M.; Cock, P.J.A.; Pritchard, L.; Cardle, L.; Shaw, P.D.; Marshall, D. Using Tablet for visual exploration of second-generation sequencing data. *Brief. Bioinform.* **2013**, *14*, 193–202. [[CrossRef](#)]
39. Quinlan, A.R.; Hall, I.M. BEDTools: A flexible suite of utilities for comparing genomic features. *Bioinformatics* **2010**, *26*, 841–842. [[CrossRef](#)]
40. Wang, Y.; Tang, H.; DeBarry, J.D.; Tan, X.; Li, J.; Wang, X.; Lee, T.-h.; Jin, H.; Marler, B.; Guo, H.; et al. MCScanX: A toolkit for detection and evolutionary analysis of gene synteny and collinearity. *Nucleic Acids Res.* **2012**, *40*, e49. [[CrossRef](#)]
41. Katoh, K.; Standley, D.M. MAFFT Multiple Sequence Alignment Software Version 7: Improvements in Performance and Usability. *Mol. Biol. Evol.* **2013**, *30*, 772–780. [[CrossRef](#)] [[PubMed](#)]
42. Huelsenbeck, J.P.; Ronquist, F. MRBAYES: Bayesian inference of phylogenetic trees. *Bioinformatics* **2001**, *17*, 754–755. [[CrossRef](#)] [[PubMed](#)]
43. Letunic, I.; Bork, P. Interactive Tree Of Life (iTOL) v4: Recent updates and new developments. *Nucleic Acids Res.* **2019**, *47*, W256–W259. [[CrossRef](#)]
44. Xia, H.; Zhao, W.; Shi, Y.; Wang, X.-R.; Wang, B. Microhomologies Are Associated with Tandem Duplications and Structural Variation in Plant Mitochondrial Genomes. *Genome Biol. Evol.* **2020**, *12*, 1965–1974. [[CrossRef](#)] [[PubMed](#)]
45. Gerke, P.; Szövényi, P.; Neubauer, A.; Lenz, H.; Gutmann, B.; McDowell, R.; Small, I.; Schallenberg-Rüdinger, M.; Knoop, V. Towards a plant model for enigmatic U-to-C RNA editing: The organelle genomes, transcriptomes, editomes and candidate RNA editing factors in the hornwort *Anthoceros agrestis*. *New Phytol.* **2020**, *225*, 1974–1992. [[CrossRef](#)]
46. Small, I.D.; Schallenberg-Rüdinger, M.; Takenaka, M.; Mireau, H.; Ostersetzer-Biran, O. Plant organellar RNA editing: What 30 years of research has revealed. *Plant J.* **2020**, *101*, 1040–1056. [[CrossRef](#)] [[PubMed](#)]
47. Zhou, S.; Zhi, X.; Yu, R.; Liu, Y.; Zhou, R. Factors contributing to mitogenome size variation and a recurrent intracellular DNA transfer in *Melastoma*. *BMC Genom.* **2023**, *24*, 370. [[CrossRef](#)]
48. Chase, M.W.; Christenhusz, M.J.M.; Fay, M.F.; Byng, J.W.; Judd, W.S.; Soltis, D.E.; Mabberley, D.J.; Sennikov, A.N.; Soltis, P.S.; Stevens, P.F.; et al. An update of the Angiosperm Phylogeny Group classification for the orders and families of flowering plants: APG IV. *Bot. J. Linn. Soc.* **2016**, *181*, 1–20.
49. Jiang, M.; Ni, Y.; Zhang, J.; Li, J.; Liu, C. Complete mitochondrial genome of *Mentha spicata* L. reveals multiple chromosomal configurations and RNA editing events. *Int. J. Biol. Macromol.* **2023**, *251*, 126257. [[CrossRef](#)] [[PubMed](#)]

50. Sloan, D.B. One ring to rule them all? Genome sequencing provides new insights into the ‘master circle’ model of plant mitochondrial DNA structure. *New Phytol.* **2013**, *200*, 978–985. [[CrossRef](#)]
51. Wang, W.; Franklin, S.B.; Ouellette, J.R. Clonal regeneration of an arrow bamboo, *Fargesia qinlingensis*, following giant panda herbivory. *Plant Ecol.* **2007**, *192*, 97–106. [[CrossRef](#)]
52. Zhang, Y.-Q.; Zhou, Y.; Hou, X.-Q.; Huang, L.; Kang, J.-Q.; Zhang, J.-Q.; Ren, Y. Phylogeny of *Fargesia* (Poaceae: Bambusoideae) and infrageneric adaptive divergence inferred from three cpDNA and nrITS sequence data. *Plant Syst. Evol.* **2019**, *305*, 61–75. [[CrossRef](#)]
53. Kim, K.H.; Lee, C.B. Socialized mitochondria: Mitonuclear crosstalk in stress. *Exp. Mol. Med.* **2024**, *56*, 1033–1042. [[CrossRef](#)] [[PubMed](#)]
54. Van Aken, O. Mitochondrial redox systems as central hubs in plant metabolism and signaling. *Plant Physiol.* **2021**, *186*, 36–52. [[CrossRef](#)] [[PubMed](#)]
55. Notsu, Y.; Masood, S.; Nishikawa, T.; Kubo, N.; Akiduki, G.; Nakazono, M.; Hirai, A.; Kadowaki, K. The complete sequence of the rice (*Oryza sativa* L.) mitochondrial genome: Frequent DNA sequence acquisition and loss during the evolution of flowering plants. *Mol. Genet. Genom.* **2002**, *268*, 434–445. [[CrossRef](#)] [[PubMed](#)]
56. Bi, C.; Qu, Y.; Hou, J.; Wu, K.; Ye, N.; Yin, T. Deciphering the Multi-Chromosomal Mitochondrial Genome of *Populus simonii*. *Front. Plant Sci.* **2022**, *13*, 914635. [[CrossRef](#)] [[PubMed](#)]
57. Yang, H.; Chen, H.; Ni, Y.; Li, J.; Cai, Y.; Ma, B.; Yu, J.; Wang, J.; Liu, C. De Novo Hybrid Assembly of the *Salvia miltiorrhiza* Mitochondrial Genome Provides the First Evidence of the Multi-Chromosomal Mitochondrial DNA Structure of *Salvia* Species. *Int. J. Mol. Sci.* **2022**, *23*, 14267. [[CrossRef](#)]
58. Yang, L.; Liu, J.; Guo, W.; Zheng, Z.; Xu, Y.; Xia, H.; Xiao, T. Insights into the multi-chromosomal mitochondrial genome structure of the xero-halophytic plant *Haloxylon Ammodendron* (C.A.Mey.) Bunge ex Fenzl. *BMC Genom.* **2024**, *25*, 123. [[CrossRef](#)] [[PubMed](#)]
59. Mower, J.P. Variation in protein gene and intron content among land plant mitogenomes. *Mitochondrion* **2020**, *53*, 203–213. [[CrossRef](#)]
60. Darracq, A.; Varré, J.-S.; Touzet, P. A scenario of mitochondrial genome evolution in maize based on rearrangement events. *BMC Genom.* **2010**, *11*, 233. [[CrossRef](#)]
61. Knoop, V. The mitochondrial DNA of land plants: Peculiarities in phylogenetic perspective. *Curr. Genet.* **2004**, *46*, 123–139. [[CrossRef](#)] [[PubMed](#)]
62. Taanman, J.-W. The mitochondrial genome: Structure, transcription, translation and replication. *Biochim. Biophys. Acta Bioenerg.* **1999**, *1410*, 103–123. [[CrossRef](#)] [[PubMed](#)]
63. Gualberto, J.M.; Newton, K.J. Plant Mitochondrial Genomes: Dynamics and Mechanisms of Mutation. *Annu. Rev. Plant Biol.* **2017**, *68*, 225–252. [[CrossRef](#)] [[PubMed](#)]
64. Han, F.; Bi, C.; Zhao, Y.; Gao, M.; Wang, Y.; Chen, Y. Unraveling the complex evolutionary features of the *Cinnamomum camphora* mitochondrial genome. *Plant Cell Rep.* **2024**, *43*, 183. [[CrossRef](#)] [[PubMed](#)]
65. McCauley, D.E. Paternal leakage, heteroplasmy, and the evolution of plant mitochondrial genomes. *New Phytol.* **2013**, *200*, 966–977. [[CrossRef](#)]
66. Hia, F.; Takeuchi, O. The effects of codon bias and optimality on mRNA and protein regulation. *Cell. Mol. Life Sci.* **2021**, *78*, 1909–1928. [[CrossRef](#)]
67. Barik, S. The Uniqueness of Tryptophan in Biology: Properties, Metabolism, Interactions and Localization in Proteins. *Int. J. Mol. Sci.* **2020**, *21*, 8776. [[CrossRef](#)] [[PubMed](#)]
68. Radrizzani, S.; Kudla, G.; Izsvák, Z.; Hurst, L.D. Selection on synonymous sites: The unwanted transcript hypothesis. *Nat. Rev. Genet.* **2024**, *25*, 431–448. [[CrossRef](#)] [[PubMed](#)]
69. Li, J.; Chen, Y.; Liu, Y.; Wang, C.; Li, L.; Chao, Y. Complete mitochondrial genome of *Agrostis stolonifera*: Insights into structure, Codon usage, repeats, and RNA editing. *BMC Genom.* **2023**, *24*, 466. [[CrossRef](#)]
70. Zardoya, R. Recent advances in understanding mitochondrial genome diversity. *F1000Research* **2020**, *9*, 270. [[CrossRef](#)]
71. Zou, Y.; Zhu, W.; Sloan, D.B.; Wu, Z. Long-read sequencing characterizes mitochondrial and plastid genome variants in *Arabidopsis msh1* mutants. *Plant J.* **2022**, *112*, 738–755. [[CrossRef](#)] [[PubMed](#)]
72. Ma, P.-F.; Zhang, Y.-X.; Guo, Z.-H.; Li, D.-Z. Evidence for horizontal transfer of mitochondrial DNA to the plastid genome in a bamboo genus. *Sci. Rep.* **2015**, *5*, 11608. [[CrossRef](#)]
73. Ala, K.G.; Zhao, Z.; Ni, L.; Wang, Z. Comparative analysis of mitochondrial genomes of two alpine medicinal plants of *Gentiana* (Gentianaceae). *PLoS ONE* **2023**, *18*, e0281134. [[CrossRef](#)] [[PubMed](#)]
74. Sloan, D.B.; Wu, Z. History of Plastid DNA Insertions Reveals Weak Deletion and AT Mutation Biases in Angiosperm Mitochondrial Genomes. *Genome Biol. Evol.* **2014**, *6*, 3210–3221. [[CrossRef](#)] [[PubMed](#)]
75. Masutani, B.; Arimura, S.; Morishita, S. Investigating the mitochondrial genomic landscape of *Arabidopsis thaliana* by long-read sequencing. *PLoS Comput. Biol.* **2021**, *17*, e1008597. [[CrossRef](#)] [[PubMed](#)]
76. He, P.; Xiao, G.; Liu, H.; Zhang, L.; Zhao, L.; Tang, M.; Huang, S.; An, Y.; Yu, J. Two pivotal RNA editing sites in the mitochondrial *atp1* mRNA are required for ATP synthase to produce sufficient ATP for cotton fiber cell elongation. *New Phytol.* **2018**, *218*, 167–182. [[CrossRef](#)] [[PubMed](#)]
77. Cheng, Y.; He, X.; Priyadarshani, S.V.G.N.; Wang, Y.; Ye, L.; Shi, C.; Ye, K.; Zhou, Q.; Luo, Z.; Deng, F.; et al. Assembly and comparative analysis of the complete mitochondrial genome of *Suaeda glauca*. *BMC Genom.* **2021**, *22*, 167. [[CrossRef](#)] [[PubMed](#)]

78. Vercellino, I.; Sazanov, L.A. The assembly, regulation and function of the mitochondrial respiratory chain. *Nat. Rev. Mol. Cell Biol.* **2022**, *23*, 141–161. [[CrossRef](#)]
79. Bi, R.; Zhang, W.; Zhang, D.-F.; Xu, M.; Fan, Y.; Hu, Q.-X.; Jiang, H.-Y.; Tan, L.; Li, T.; Fang, Y.; et al. Genetic association of the cytochrome c oxidase-related genes with Alzheimer’s disease in Han Chinese. *Neuropsychopharmacology* **2018**, *43*, 2264–2276. [[CrossRef](#)]
80. Analin, B.; Mohanan, A.; Bakka, K.; Challabathula, D. Cytochrome oxidase and alternative oxidase pathways of mitochondrial electron transport chain are important for the photosynthetic performance of pea plants under salinity stress conditions. *Plant Physiol. Biochem.* **2020**, *154*, 248–259. [[CrossRef](#)]

Disclaimer/Publisher’s Note: The statements, opinions and data contained in all publications are solely those of the individual author(s) and contributor(s) and not of MDPI and/or the editor(s). MDPI and/or the editor(s) disclaim responsibility for any injury to people or property resulting from any ideas, methods, instructions or products referred to in the content.